Hindawi Publishing Corporation
Advances in Materials Science and Engineering
Volume 2015, Article ID 859069, 7 pages
http://dx.doi.org/10.1155/2015/859069

Research Article

Influence of Alternation of Sulfate Attack and Freeze-Thaw on Microstructure of Concrete

Huaquan Yang,[1] Xiaoming Shen,[2] Meijuan Rao,[1] Xiang Li,[1] and Xiaodong Wang[3]

[1]*Changjiang River Scientific Research Institute, Wuhan 430010, China*
[2]*State Key Laboratory of Water Resources and Hydropower Engineering Science, Wuhan University, Wuhan 430072, China*
[3]*School of Engineering, College of Physical Sciences, University of Aberdeen, Aberdeen AB24 3UE, UK*

Correspondence should be addressed to Meijuan Rao; raomeijuanding@163.com

Received 30 April 2015; Revised 7 July 2015; Accepted 8 July 2015

Academic Editor: Antônio G. B. de Lima

The effects of sulfate attack and freeze-thaw alternation on the concrete microstructure were systemically investigated by advanced test methods such as water absorption method, air void analysis, XRD, and SEM. The experimental results indicated that freeze-thaw damage is the major effective factor in the sulfate attack and freeze-thaw alternation test. In the alternation test, average aperture of capillary pores of specimens was smaller, pores uniformity was better, and water absorption rate was lower than those specimens used in the single freeze-thaw damage test. The average aperture and uniformity of pores could be improved by adding fly ash and slag. Damage was accumulated in many cycles of freeze-thaw and microcracks increased during the test. At the same time, the hydration products of the concrete developed into expansive gypsum, AFt, and TSA without any strength during sulfate attack. The results of the microstructure analysis form XRD and SEM are in accordance with that of AFt, about 3 μm length, around which other hydration products decomposed by C-S-H after sulfate attack resulted in loss of concrete strength.

1. Introduction

Sulfate attack and freeze-thaw damage are two kinds of adverse environmental problems that hydraulic concrete engineering often encounter [1–4] and also the main problem of concrete aging diseases, especially in cold areas of the world. Hydraulic concrete structures in the cold regions often suffer from freeze-thaw damage, such as hydraulic concrete structure in areas of changes in water level, the pool, the power station cooling tower, and roads in contact with water [5, 6]. In Northeast China, North China, and Northwest China, almost all the hydraulic structures are subjected to freeze-thaw damage, locally or in large areas [7–10].

A typical engineering station, Yunfeng hydropower station, has greatly suffered from freeze-thaw damage. The damaged surface area of the spillway dam was up to 10000 m^2 (about 50% of the whole area) during less than 10 years in operation. The average depth of the freeze-thaw erosion to the concrete was more than 10 cm. Some examples of damage caused by sulfate attack have occurred in the coastal areas all over the world. At present, sulfate attack is mainly due to two factors: one is the groundwater environment and the other is the discharge of industrial wastewater [11–15].

In recent years, researchers home and abroad have attached great importance to the study of concrete durability, and a large number of systemic tests have been conducted in the study of single factor damage on concrete, and a lot of achievements have been reached [16, 17]. However, the concrete durability in real engineering environments is often a complex problem affected by multiple factors rather than merely a single one. Service engineering concrete can be affected by environmental factors, climatic conditions, and loads, whereas the interactions of these may further influence the durability of concrete [18–20]. Therefore, it is essential to study the durability of concrete under conditions with more than a single damaging factor. There is currently however a dearth of literature dealing with such systems. In this work, we report for the first time the effects of multiple detrimental factors on concrete durability, taking sulfate erosion and freeze-thaw damage as two representative factors.

Table 1: Chemical and physical properties of cement, fly ash, and slag.

	Chemical composition/%										Physical properties	Compressive strength of cement/MPa	
	SiO_2	Al_2O_3	Fe_2O_3	CaO	MgO	K_2O	Na_2O	R_2O	SO_3	loss	Specific density /(kg/m^3)	7 days	28 days
Cement	22.53	3.89	4.88	63.00	2.09	0.50	0.09	0.42	2.08	0.59	3120	25.4	45.1
Fly ash	52.44	24.03	9.44	3.20	1.14	—	—	—	0.73	2.24	2380	—	—
Slag	33.67	14.60	1.72	34.67	9.89	0.65	0.27	—	1.95	2.38	2860	—	—

Table 2: Mix proportions of concrete.

Samples	W/C	Fly ash (%)	Slag (%)	Admixture		Slump (mm)	Air content (%)	Compressive strength/MPa
				GYQ (%)	JM-II (%)			28 d
SX-1	0.40	0	0	0.008	0.7	13	5.4	37.93
SX-2	0.40	20	0	0.008	0.7	38	3.5	36.88
SX-3	0.40	0	20	0.008	0.7	40	5.4	38.29

Table 3: Mix of paste.

Samples	Cementitious materials (%)			W/C
	Cement	Fly ash	Slag	
1	100	0	0	0.50
2	80	20	0	0.50
3	80	0	20	0.50

2. Experimental

2.1. Raw Materials. Cement 42.5 used in this work was supplied by Shimeng Cement Co., Ltd. (Hunan Province, China). The pertinent physical and chemical properties of the cement were obtained from Changjiang River Scientific Research Institute. Fly ash from Power Plant of Qujing and slag powder from Wuhan Iron and Steel Co., Ltd. used are listed in Table 1. Natural fine sand with size of 0.16–0.63 mm and specific gravity of 2.65 was used as a fine aggregate.

For each mixture, the elected components were mixed, cast, and vibrated in 6 sequences as 100 mm × 100 mm × 100 mm concrete specimen. Specimens were demolded after 24 h of casting and cured with a condition of 20 ± 3°C and 95% relative humidity until the age of testing.

2.2. Test Methods. The curing ages of the specimens were 7 days and 28 days, respectively, before testing. The mix proportion of concrete specimens is shown in Table 2 and paste specimens in Table 3. Sulfate attack test was carried out in accordance with GB/T50082-2009. The specimens were immersed in 5% Na_2SO_4 solution for 16 h, then dried in an oven at 80°C for 6 h, and finally cooled in air for 2 h. This is called a sulfate attack cycle.

Freeze-thaw cycles were carried out in accordance with GB/T5150-2001. The temperature of the sample center ranged from −18.0 ± 2.0°C to 5.0 ± 2.0°C Sulfate attack and freeze-thaw alternation cycle is the alternation between the two tests. Specimens were subjected to 30 sulfate attack cycles and then 50 freeze-thaw cycles were carried out. This constitutes an alternation cycle.

The paste samples expansion ratio test was conducted based on GB/T749-2008. Adding a certain amount of dihydrate gypsum made the weight content of the SO_3 in cement and dihydrate gypsum to 7%. 25 mm × 25 mm × 280 mm paste specimen cured in water first for 30 min was measured as the initial specimen length L_0. The specimen expansion ratio P_n is formulated as (1) and L_n is the length of specimen cured n days:

$$P_n = \frac{(L_n - L_0) \times 100}{250}. \quad (1)$$

The water absorption kinetics method was conducted based on the ASTM C 642-06 Standard: Under isothermal conditions (20°C), when the wool stoma absorption occurs in mortar, concrete, and other materials, the water sorption curve has a characteristic of an exponential function, and so their pore structure analysis using water absorption kinetics can be carried out. The weight of 100 mm × 100 mm × 100 mm concrete specimens, cured to the specified age, which are dried in an oven at 105°C for 24 h and cooled in air to normal temperature, was recorded as m_0. The dried specimens were then immersed in water for 0.25 h, with weight in air measured as $m_{0.25}$, and in the same way, m_1 and m_{24} are recorded. Finally, the weight in water is measured and recorded as m'_{24}. The weight water absorption rate (W_G) is formulated as

$$W_G = \frac{m_{24} - m_0}{m_0} \cdot 100\%. \quad (2)$$

The volume water absorption rate (W) is formulated as

$$W = \frac{m_{24} - m_0}{m_{24} - m'_{24}} \cdot 100\%. \quad (3)$$

Bubble structures test could measure the pore structure of concrete. The test was performed on the Rapid Air 457 Air void analyzer (Concrete Experts International). The concrete specimens were dried at 60°C and then cut into pieces for the test.

After drying and grinding into powder, pure cement paste was investigated by X-ray diffraction (XRD) to study

Table 4: Expansion ratio of paste samples.

Samples	Expansion ratio in water				Expansion ratio in Na_2SO_4 solution			
	7 d	28 d	90 d	180 d	7 d	28 d	90 d	180 d
1	0	11	58	36	4	76	200	328
2	2	22	48	24	8	124	212	300
3	8	36	84	72	16	124	208	272

Table 5: Water absorption kinetics parameters of concrete samples.

Samples	Volumetric water absorption rate W (%)				Compressive strength/MPa			
	WA	FR	SU	AL	WA	FR	SU	AL
SX-1	3.0	7.0	3.5	5.9	54.75	41.99	47.12	40.28
SX-2	4.1	8.3	2.6	4.3	54.56	43.92	48.73	42.55
SX-3	4.1	6.9	4.1	4.5	54.89	44.51	50.52	43.08

Notification: WA: water; FR: freeze; SU: sulfate; AL: alternation.

the change of reaction products after sulfate attack. Phase analysis was conducted using X-ray Diffraction machine (scan interval 5–60° 2θ) produced by Bruker. X-ray tube accelerating voltage was 60 kV, rotating anode was 3 kW, and goniometer table was 200 mm.

Cement paste in concrete specimens was investigated by scanning electron microscope (SEM) to analyze the microstructure of concrete after the alternation of sulfate attack and freeze-thaw test. JSM-5610LV scanning electron microscope was produced by JEOL. Resolution ratio was 3 nm and enlargement factor was from 18 to 300000.

3. Results and Discussion

3.1. Expansion Ratio Analysis. Paste samples cured in water and Na_2SO_4 solution were used to analyze the expansion ratio, where the results are shown in Table 4.

The results demonstrated that expansion ratios of paste samples cured in Na_2SO_4 solution were significantly greater than those cured in water, and expansion ratios increased by cure age. This indicates that the expansive substance is produced by hydration products reacting with Na_2SO_4 solution. The activity of admixture could be motivated while specimens were cured in Na_2SO_4 solution more than 100 days; at the same time, sulfate erosion resistant ability of concrete would be arisen gradually, $Ca(OH)_2$ be consumed by secondary hydration, and tricalcium aluminate be decreased through physical dilution. The reason is that expansive product like ettringite was reacted between Na_2SO_4 solution and dihydrate gypsum in paste samples. Meanwhile, cement hydration products like $Ca(OH)_2$ and hydrated calcium aluminate reacted to produced gypsum and ettringite. Expansion ratio of specimen cured in Na_2SO_4 solution grew rapidly since bulk increase of erosion products.

3.2. Water Absorption Kinetics Analysis. Concrete samples prepared by four alternation times of sodium sulfate erosion and freeze-thaw, 200 times' freeze-thaw only, and 120 days' alternation of sodium sulfate erosion were used to analyze the results as shown in Table 5 and Figure 1.

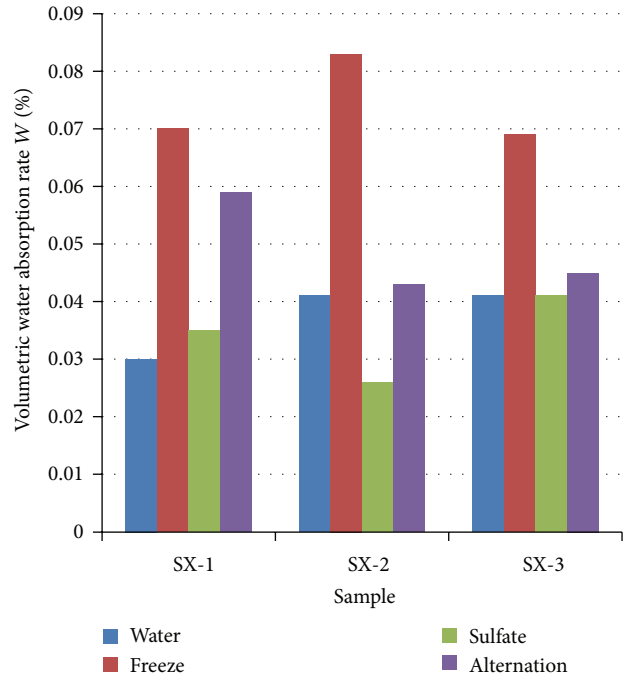

Figure 1: Volumetric water absorption of concrete.

The results showed that freeze-thaw was the main factor in the alternate destruction. In contrast with concrete cured in water, after the specimens were damaged by freeze-thaw, the volumetric water absorption increased significantly, but with no great contribution to the pore size uniformity. After the concrete was eroded by sodium sulfate, volumetric water absorption did not change much.

After the alternation of sodium sulfate erosion and freeze-thaw, the concrete volumetric water absorption rate is larger than one eroded by sodium sulfate while smaller than one

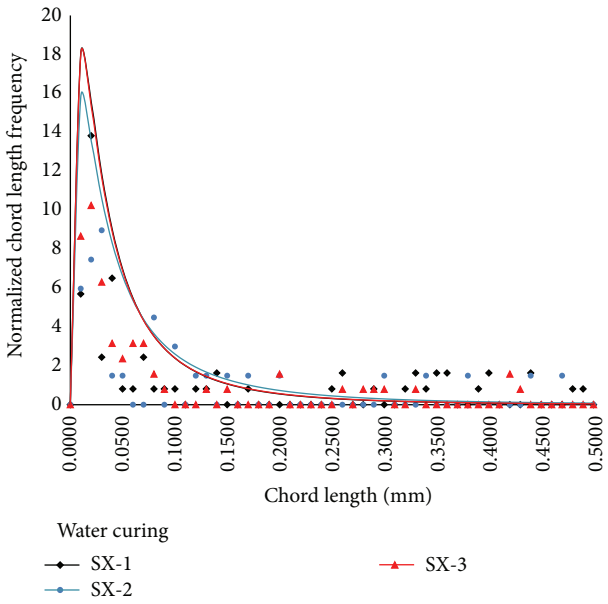

Figure 2: Bubbles normal distribution curves of samples curing in water.

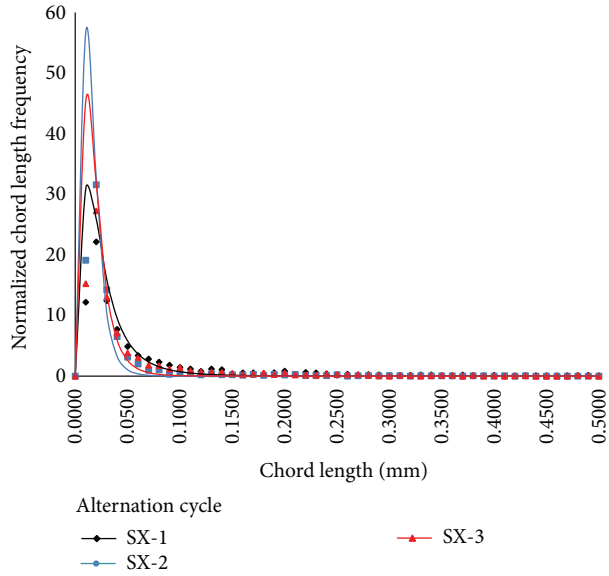

Figure 3: Bubbles normal distribution curves of samples under four times' alternation of sodium sulfate erosion.

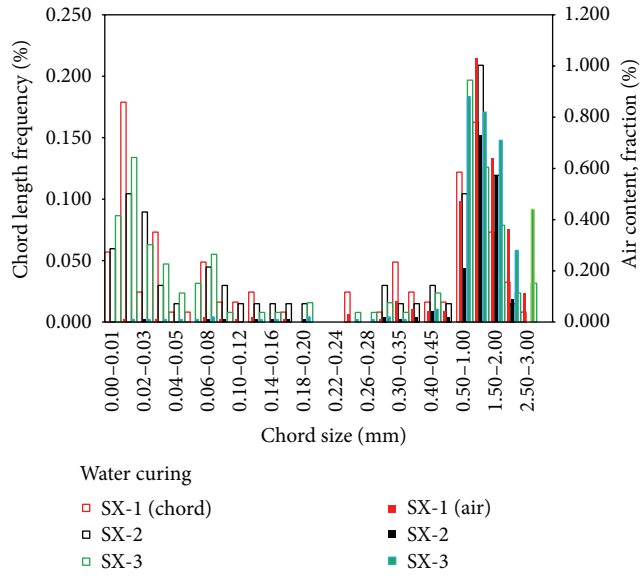

Figure 4: Bubbles distribution law curves of samples curing in water.

damaged by freeze-thaw. This indicates that the corrosive substance produced by hydration products reacting with sodium sulfate would fill part of concrete pores.

From the view point of admixture, the volumetric water absorption of concrete with admixture was smaller than the concrete without admixture.

The compressive strength of concrete as shown in Table 5 is in good agreement with the above analysis. After the alternation of sodium sulfate erosion and freeze-thaw, the compressive strength of the concrete was lower than that of the concrete eroded by single damage. Freeze-thaw was the main factor during the alternate destruction. Moreover, the compressive strength of the concrete after freeze-thaw damage decreased more than the samples eroded by sodium sulfate. It is noteworthy that fly ash and slag powder may improve the compressive strength, where the improving effect of slag powder was better than that of fly ash.

3.3. Bubble Structure Analysis. The concrete samples cured in water for 28 days were used for the pore structure experiments. The pore parameters are shown in Table 5. The normal distribution of bubbles and bubbles distribution law of samples cured in water are shown in Figures 2 and 4, while the results of samples after four alternation times of sodium sulfate erosion and freeze-thaw are shown in Figures 3 and 5.

3.3.1. Air Content. After four alternation times of sodium sulfate erosion and freeze-thaw, the air content of the concrete increased, and the air content of concrete without admixture was greater than that of concrete containing fly ash and slag powder, respectively. This was consistent with the change in the concrete compressive strength. Also, the pore structure results were the same as those obtained in the water absorption kinetics pore structure test.

The slurry air ratio is also closely related to the mechanical properties of the concrete. Usually, the larger the slurry air ratio, the higher the concrete strength. Repeated freeze-thaw cycle accumulated the damage effect as well as the fatigue effect and made the freezing generated microfissures expand. The increased porosity weakened the resistance of the concrete and increased its water absorption as well.

The sodium sulfate erosion made the hydration products of the concrete like gypsum and ettringite expand and calcium sulfur rankinite without strength. This made the concrete material to suffer greater damage in the next frozen damage, with its resistance reducing more as the damage

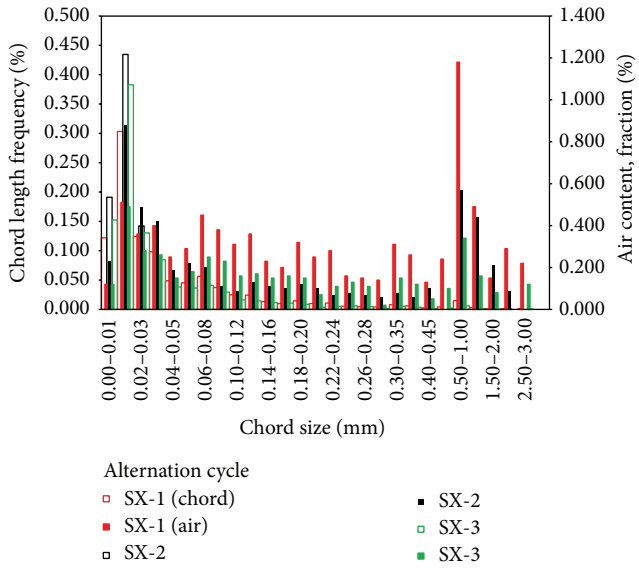

Figure 5: Bubbles distribution law curves of samples under four times' alternation of sodium sulfate erosion.

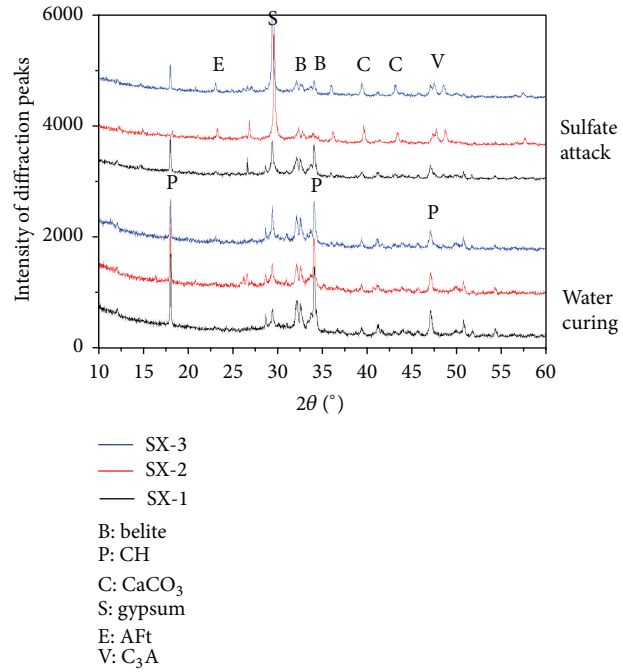

Figure 6: X-ray diffraction (XRD) analysis of samples SX-1, SX-2, and SX-3.

becomes more severe. The porosity also increased more as well. Again and again, under the alternation of freeze-thaw, a vicious circle was formed, making the concrete durability decline gradually.

3.3.2. Spacing Factor. The spacing factor of the concrete was high before erosion and freeze-thaw. The spacing factors of the samples SX-1, SX-2, and SX-3 were 0.744 mm, 1.035 mm, and 0.771 mm, respectively. The "SX" represents the name of the serial number. However, the spacing factor of the samples decreased significantly to 0.040 mm, 0.034 mm, and 0.052 mm, respectively, after erosion. As the air content became bigger, the spacing factor became smaller, which indicated that there was a fine corresponding relationship between the spacing factor and the air content of the concrete.

3.3.3. Bubbles Distribution. The effect of bubbles on concrete properties cannot be simply evaluated by air content. Actually, the bubbles distribution conditions (bubbles structure) including the size, amount, and distribution are more important. The size and distribution would greatly differ from each other when the air content is the same in the concrete.

The bubble chord length in concrete is between 10 microns and 0.5 mm. There is also a part of the chord as large as 3 mm. When soaked in water for 28 days, the chord which was less than 0.5 mm in length in specimen SX-1 increased to 74, accounting for about 60.2% of the total length and the chord which was less than 1 mm in length in specimen SX-1 also increased to 89, accounting for 72.4% of the total. However, the bubble parameters of the concrete containing admixture changed a little. After 4 alternation times of sodium sulfate erosion and freeze-thaw, the internal chord length in concrete specimen SX-1 less than 0.5 mm increased rapidly, up to 2741, accounting for 97.9% of the total and the number of the chord lengths less than 1 mm increased to 2783, accounting for 99.4%. The above data indicate that, after the concrete has gone through the alternation of sodium sulfate and freeze-thaw, the internal chord structure changes greatly. The concrete with porous structure produces more pores after injury. Although the number of chords less than 0.5 mm in length accounts for larger proportion after alternation; the number of chord lengths between 0.5 mm and 1 mm increased by 27% due to the increase in the total number. This is consistent with the water absorption kinetics where, after alternation, the water absorption increases significantly.

3.4. XRD Analysis. After curing in water, the pure cement paste without admixture had strong $Ca(OH)_2$ diffraction. However, after the sodium sulfate erosion for 120 days, the $Ca(OH)_2$ diffraction intensity decreased and diffractions of $CaCO_3$ and $CaSO_4 \cdot 2H_2O$ were produced. As shown in Figure 3, after curing in water, the hydration products of pure cement paste containing 20% fly ash were similar to the specimen with no admixture. Similarly, after the specimen was eroded by sulfate, the diffraction intensity of $Ca(OH)_2$ decreased, whereas obvious low temperature quartz Aft diffraction and strong $Ca(OH)_2$ diffraction were produced. As shown in Figure 6, after curing in water, the $Ca(OH)_2$ diffraction in hydration products of cement paste specimen containing 20% slag was lower than the two former kinds. Also, after the specimen was eroded by sulfate, strong diffraction intensity of $CaSO_4 \cdot 2H_2O$ and a little Aft diffraction were produced.

The above observations show that the main hydration product of cement is $Ca(OH)_2$ crystal. After sulfate erosion, large amount of corrosive products such as gypsum and

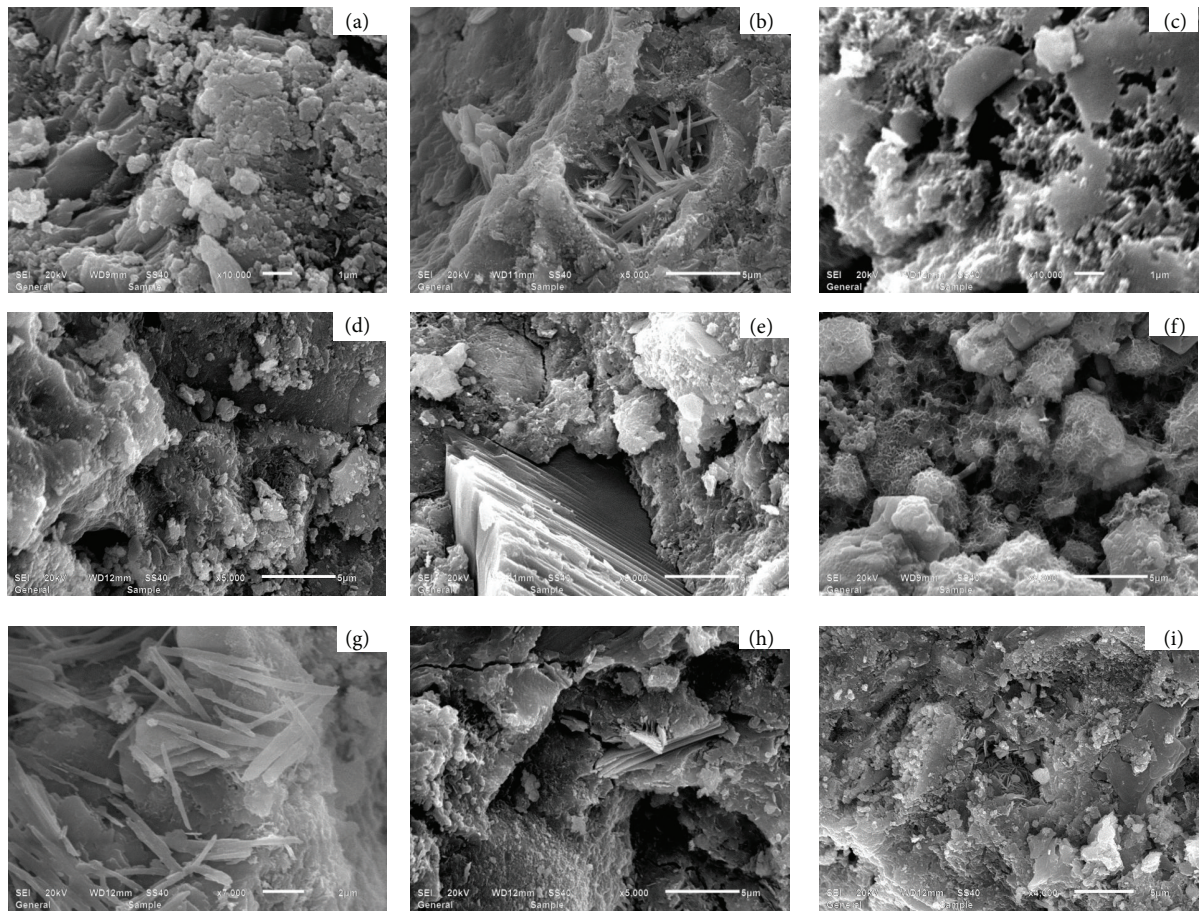

Figure 7: SEM images of samples (((a), (b), (c)) erosion in 5% sodium sulfate solution for 120 days; ((d), (e), (f)) two hundred times' freeze-thaw; ((g), (h), (i)) four times' erosion freeze-thaw alternation).

ettringite were mainly produced. This shows that the specimen is mainly eroded by plaster mold sulfate, which leads to the formation of the main hydration product, C-S-H gel on the surface of the cement paste specimen decomposing directly, softening the specimen surface, forming a plasma phenomenon, and eventually resulting in loss of strength.

3.5. SEM Analysis. The SEM images of concrete erosion in 5% sodium sulfate solution for 120 days, two hundred times freeze-thaw, and four times erosion-freeze-thaw alternation are shown in Figure 7.

After the sodium sulfate erosion, the structure is poorly cemented with slight cracks inside which there were hydration products. In addition, there were many hydration products on the fly ash particles, and its surrounding appeared as ettringite of about 3 μm, which was consistent with the XRD conclusion above. However, after the freeze-thaw cycles, the structure was very loose, and a large number of cracks were produced. The pellet feeling was enhanced in the concrete containing slag, and a large amount of linked network structure products was generated on the surface.

After alternation of sodium sulfate erosion and freeze-thaw, the structure was very loose with cracks and pores production. The ettringite with length and width of about 5 and 0.5 μm, respectively, was produced. Compared with the specimen after sodium sulfate erosion only, the ettringite had larger length and width, which indicates that freeze-thaw damage promoted chemical reactions between sodium sulfate and hydration products. In addition, it could be seen from the concrete containing fly ash that the fly ash spherical surface was no longer smooth due to a large amount of hydration products and the concrete containing slag was more compact compared with the two former kinds. Also six-party plate type single sulfur hydrated calcium sulphoaluminate (AFm) with the size of about 1 μm was produced. These microscopic test results show that hydration products and internal structure change when the concrete is launched in different environment and can be well explained by the microstructure features and the XRD results.

4. Conclusions

(1) Between the alternation of sodium sulfate erosion and freeze-thaw, freeze-thaw damage was the main factor which made the bubble inside the concrete to become larger and provided a better reaction space for the concrete hydration products and the sodium sulfate reaction. Corrosive products, like gypsum, ettringite,

and so forth, were produced in the reaction. Corrosive products made the specimens expansive. Due to short reaction time, the corrosive substances filled part of the pores. After alternation, the bubbles became bigger with increasing bubble number and also the production of a great deal of expansive materials.

(2) After alternation of sodium sulfate erosion and freeze-thaw, ettringite inside the concrete was longer and wider than that simply eroded by sodium sulfate. In addition, the internal structure of the concrete became looser and cracks grew, indicating that freeze-thaw promoted sodium sulfate erosion.

(3) As for the concrete containing 20% fly ash or slag powder, due to the filling effect and microaggregate effect, the average pore size and size uniformity of bubbles were improved. The density of the hydration system was also increased when the proper admixture was added. Otherwise, the improvement degree of concrete microstructure containing fly ash was larger than slag. The hydration products of concrete were similar among the concrete without admixture, concrete containing 20% fly ash, and concrete containing 20% slag. After the sodium sulfate erosion, the gypsum diffraction intensity was not strong, and the sample may be the reason; the materials produced by concrete containing fly ash or slag powder were also similar.

Conflict of Interests

The authors declare that there is no conflict of interests regarding the publication of this paper.

Acknowledgment

The authors were supported by the National Natural Science Foundation of China Projects (51279017 and 51139001).

References

[1] S. U. Al-Dulaijan, M. Maslehuddin, M. M. Al-Zahrani, A. M. Sharif, M. Shameem, and M. Ibrahim, "Sulfate resistance of plain and blended cements exposed to varying concentrations of sodium sulfate," *Cement and Concrete Composites*, vol. 25, no. 4-5, pp. 429–437, 2003.

[2] P. J. Tikalsky and R. L. Carrasquillo, "Influence of fly ash on the sulfate resistance of concrete," *ACI Materials Journal*, vol. 89, no. 1, pp. 69–75, 1992.

[3] O. S. B. Al-Amoudi, M. Maslehuddin, and Y. A. B. Abdul-Al, "Role of chloride ions on expansion and strength reduction in plain and blended cements in sulfate environments," *Construction and Building Materials*, vol. 9, no. 1, pp. 25–33, 1995.

[4] J. Hill, E. A. Byars, J. H. Sharp, C. J. Lynsdale, J. C. Cripps, and Q. Zhou, "An experimental study of combined acid and sulfate attack of concrete," *Cement and Concrete Composites*, vol. 25, no. 8, pp. 997–1003, 2003.

[5] H. T. Cao, L. Bucea, A. Ray, and S. Yozghatlian, "The effect of cement composition and pH of environment on sulfate resistance of Portland cements and blended cements," *Cement and Concrete Composites*, vol. 19, no. 2, pp. 161–171, 1997.

[6] E. E. Hekal, E. Kishar, and H. Mostafa, "Magnesium sulfate attack on hardened blended cement pastes under different circumstances," *Cement and Concrete Research*, vol. 32, no. 9, pp. 1421–1427, 2002.

[7] O. S. B. Al-Amoudi, "Sulfate attack and reinforcement corrosion in plain and blended cements exposed to sulfate environments," *Building and Environment*, vol. 33, no. 1, pp. 53–61, 1998.

[8] Y.-S. Park, J.-K. Suh, J.-H. Lee, and Y.-S. Shin, "Strength deterioration of high strength concrete in sulfate environment," *Cement and Concrete Research*, vol. 29, no. 9, pp. 1397–1402, 1999.

[9] E. Grabowski, B. Czarnecki, J. E. Gillott, C. R. Duggan, and J. F. Scott, "Rapid test of concrete expansivity due to internal sulfate attack," *ACI Materials Journal*, vol. 89, no. 5, pp. 469–480, 1992.

[10] H. Lee, R. D. Cody, A. M. Cody, and P. G. Spry, "Reduction of concrete expansion by ettringite using crystallization inhibition techniques," *Environmental and Engineering Geoscience*, vol. 9, no. 4, pp. 313–326, 2003.

[11] R. Tixier and B. Mobasher, "Modeling of damage in cement-based materials subjected to external sulfate attack. II: comparison with experiments," *Journal of Materials in Civil Engineering*, vol. 15, no. 4, pp. 314–322, 2003.

[12] M. D. Cohen and B. Mather, "Sulfate attack on concrete: research needs," *ACI Materials Journal*, vol. 88, no. 1, pp. 62–69, 1991.

[13] T. C. Powers, "A working hypothesis for further studies of frost resistance of concrete," *Journal of the American Concrete Institute*, vol. 16, no. 4, pp. 245–272, 1945.

[14] L. Jiang, D.-T. Niu, Y.-Z. Sun, and Q.-N. Fei, "Ultrasonic testing and microscopic analysis on concrete under sulfate attack and cyclic environment," *Journal of Central South University*, vol. 21, no. 12, pp. 4723–4731, 2014.

[15] J. Stroh, M.-C. Schlegel, E. F. Irassar, B. Meng, and F. Emmerling, "Applying high resolution SyXRD analysis on sulfate attacked concrete field samples," *Cement and Concrete Research*, vol. 66, pp. 19–26, 2014.

[16] G. Long, Y. Xie, and X. Tang, "Evaluating deterioration of concrete by sulfate attack," *Journal Wuhan University of Technology, Materials Science Edition*, vol. 22, no. 3, pp. 572–576, 2007.

[17] Z. Liu and D. Deng, "Physicochemical study on the interface zone of concrete exposed to different sulfate solutions," *Journal of Wuhan University of Technology—Materials Science Edition*, vol. S1, pp. 167–174, 2006.

[18] D. Niu, L. Jiang, and Q. Fei, "Deterioration mechanism of sulfate attack on concrete under freeze-thaw cycles," *Journal of Wuhan University of Technology—Materials Science Edition*, vol. 28, no. 6, pp. 1172–1176, 2013.

[19] C. Yu, W. Sun, and S. Karen, "Application of image analysis based on SEM and chemical mapping on PC mortars under sulfate attack," *Journal of Wuhan University of Technology-Materials Science Edition*, vol. 29, no. 3, pp. 534–539, 2014.

[20] Z. Baščarević, M. Komljenović, Z. Miladinović, V. Nikolić, N. Marjanović, and R. Petrović, "Impact of sodium sulfate solution on mechanical properties and structure of fly ash based geopolymers," *Materials and Structures*, vol. 48, no. 3, pp. 683–697, 2014.